Articular Cartilage Zonal Differentiation via 3D Second Harmonic Generation Imaging Microscopy

Rajeev Chaudhary[1,2], **Kirby R. Campbell**[1,3], **Karissa B. Tilbury**[1,3], **Ray Vanderby Jr.**[1,2], **Walter F. Block**[1,4,5], **Richard Kijowski**[5], and **Paul J. Campagnola**[1,3,4,*]

[1]Department of Biomedical Engineering, University of Wisconsin-Madison, Madison, WI

[2]Department of Orthopedics & Rehabilitation, University of Wisconsin-Madison, Madison, WI

[3]Department of Laboratory for Optical and Computational Instrumentation, University of Wisconsin-Madison, Madison, WI

[4]Department of Medical Physics, University of Wisconsin-Madison, Madison, WI

[5]Department of Radiology, University of Wisconsin-Madison, Madison, WI

Abstract

Purpose—The collagen structure throughout the patella has not been thoroughly investigated by 3D imaging, where the majority of the exiting data comes from histological cross sections. It is important to have a better understanding of the architecture in normal tissues, where this could then be applied to imaging of diseased states.

Methods—To address this shortcoming, we investigated the combined use of collagen specific Second Harmonic Generation (SHG) imaging and measurement of bulk optical properties to characterize collagen fiber orientations of the histologically defined zones of bovine articular cartilage. Forward and backward SHG intensities from sections from superficial, middle and deep zones were collected as a function of depth and analyzed by Monte Carlo simulations to extract the SHG creation direction, which is related to the fibrillar assembly.

Results—Our results revealed differences in SHG forward-backward response between the three zones, where these are consistent with a previously developed model of SHG emission. Some of the findings are consistent with that from other modalities; however, SHG analysis showed the middle zone had the most organized fibril assembly. While not distinct, we also report bulk optical property values for these different zones within the patella.

Conclusions—Collectively, these results provide quantitative measurements of structural changes at both the fiber and fibril assembly of the different cartilage zones and reveals structural information not possible by other microscope modalities. This can provide quantitative insight to the collagen fiber network in normal cartilage, which may ultimately be developed as a biomarker for osteoarthritis.

[*]Corresponding author: pcampagnola@wisc.edu.

Declaration of Interests: We have no conflicts of interest to declare.

Keywords

Cartilage; Second Harmonic Generation; Collagen; scattering; 3D; microscopy

Introduction

Articular cartilage is one of the most important soft tissues in the body as it assists in movement and transmission of loads across joints smoothly with little friction, yet the architecture of the collagen fiber network is still not well defined across its histological zones (1-3). For examples, collagen content decreases only by about 5% during the early stages of disease such as osteoarthritis (OA), but the corresponding changes in collagen fiber orientation are not well characterized or quantified (4-9). In order to better identify the sequence of events that occur during cartilage degeneration, it is essential to first understand the structure, morphology and orientation of the collagen fiber network in mature, healthy cartilage.

In normal articular cartilage, 90% of the collagen content is type II collagen (Col II), however within the Col II fibers other collagen isoforms (IX, and XI) fibrils are co-mingled to form fibers dictating the tissue anisotropy of articular cartilage (3). The spatial distribution of the collagen and chondrocytes, as shown through histological methods, tends to be fairly uniform throughout much of the extracellular matrix (ECM; see Figure 1 for cartoon); however, the collagen content relative to cell distribution in the middle zone is quite heterogeneous and not well characterized. Previous microscopic techniques utilized polarized light microscopy (PLM) and electron microscopy (EM) to analyze cartilage ultrastructure. PLM may yield good structural information in terms of alignment, but it provides poor 3D sectioning, penetration depth, molecular structure, and chemical specificity (10-12). EM provides high-resolution images of ultrastructure but is limited by sample size, difficult sample preparation, and poor signal-to-noise ratio (SNR) due to the limited, tolerable electron doses for biologic samples (13-15). Both of these techniques require harmful sample preparation such as paraffin or resin embedding, which limits the effective use in assessment as well as the volume of tissue that can be imaged.

Second Harmonic Generation (SHG) imaging microscopy may be a superior tool in quantifying the changes in collagen distribution and orientation throughout the cartilage extracellular matrix (ECM). SHG is a second-order, nonlinear optical process that can acquire three-dimensional, sub-micron resolution images of non-centrosymmetric assemblies, such as collagen fibers in the cartilage ECM (10, 16-18). SHG is a coherent process in which two photons simultaneously induce a second order polarization in a tissue and emit a photon of exactly twice the frequency, governed by:

$$\overrightarrow{P} = \chi^{(2)} \overrightarrow{E} \cdot \overrightarrow{E}, \quad (1)$$

where P is the induced polarization, E is the electric field vector of the laser, and $\chi^{(2)}$ is the second order nonlinear susceptibility tensor of collagen, which is the bulk property that determines the contrast in the microscope (19). Due to the second order symmetry constraints imposed by $\chi^{(2)}$ on the harmonophores and their assemblies, the SHG contrast

increases for well-ordered structures; however, it vanishes for assemblies with a center of inversion symmetry (19, 20). Therefore, the magnitude of $\chi^{(2)}$ that is experimentally manifested in the SHG intensity reflects the relative alignment of collagen fibers and their concentration (21). This tensor can also be analyzed to yield macromolecular structural data, including the α-helix pitch angle and the alignment of dipole moments with fibrils (10, 16, 17, 20, 22).

An added benefit of SHG resides in its physically determined emission direction that contains information related to the fibril architecture (23-26). We note that this is in stark contrast to the more common two-photon excitation fluorescence (TPEF) whose emission is spatially isotropic. The SHG process is governed by specific phase matching considerations as the emitted SHG directionality is different between most tissues as well as the traditional models of uniaxial crystals (17). For example, SHG is perfectly phase matched in a uniaxial crystal, where:

$$\Delta k = k_{2\omega} - 2k_{\omega} = 0, \quad \text{(2)}$$

where k_{ω} and $k_{2\omega}$ are the wavevectors for the incident photon, and the SHG emission, respectively. This SHG emission in a perfectly phase matched system is 100% forward directed. In contrast, in biological tissues there is an inherent randomness and dispersion which results in a nonzero k distribution, i.e. a distribution of values that are not perfectly phase matched (23). To conserve momentum, a distribution of forward and backward components must then occur and we denote these components F_{SHG} and B_{SHG}. We have previously shown how the ratio is related to the sub-resolution fibril organization (23). Specifically, in the axial direction, structures much smaller than λ_{SHG} result in nearly equal forward and backward components, whereas structures on the order of λ_{SHG} yield primarily forward directed SHG (17, 23).

Currently, there have only been a few studies using SHG on articular cartilage (27-32). Most of this work only utilized backward propagating SHG due to its ease of detection with minimal microscope modifications, whereas most of the signal is forward directed. Furthermore, the use of both components yields additional information as described above (27, 28, 33, 34). Additionally, many of these studies used thin human cartilage sections (~10-25 μm), embedded the tissue in paraffin, and imaged in the sagittal plane to characterize each zone as seen previously in the gold standard of histology. More recently, work from Dumas (35), Davies (30), and Légaré (32) have used forward SHG to model the collagen architecture of articular cartilage. Collectively, the results from these prior studies suggest that cartilage structure and orientation can be determined through SHG; however, structural aspects have not yet been fully determined (27-32). The purpose of our study is to investigate the sensitivity of SHG directional (forward-backward) measurements and bulk optical properties to characterize collagen architecture in different histological zones of axially-sliced articular cartilage as well as obtain optical property measurements of these zones, which are also reflective of collagen architecture. The SHG specific methods go beyond simple morphological analysis and are thus generalizable to essentially any tissue, regardless of its specific morphology and alignment (or lack thereof) Moreover, our attempts at using standard analysis tools of morphology were not successful in delineating these

zones due to the non-discrete nature of Col II fibers. We suggest that the SHG and optical property metrics could be different in diseased states such as OA.

Materials and Methods

Sample Preparation

Fresh bovine knee joints were obtained from a local abattoir (Black Earth Meats; Black Earth, WI). A fresh bovine patella specimen was excised from three, skeletally mature cows, 24 to 30 months of age. Careful handling of each patella with a diamond blade band saw ensured bone was properly removed in order to provide a flat cartilage surface for analysis. Plugs of seven mm in diameter (non-decalcified) were taken from the central portion of each patellar surface, and each cartilage plug was sectioned into 100 μm thick, axial sections from the superficial to deep layers, using a vibratome (Leica; Wetzlar, Germany). Samples were acquired from 3 different animals, and these were cut in 100 μm thick sections from the surface to the bone. Sections were fixed in 10% neutral buffered formalin for three incubation periods of 15 minutes and multiple phosphate-buffered saline (PBS) washes. Specimens were stored in PBS at 4°C prior to SHG imaging for no more than one week post-mortem. We note that these measurements were performed on fixed tissues, but previous EM studies have revealed that fixation does not result significantly alter the collagen fibrillar structure and only results in a small volume loss of about 20% (36). We have also compared SHG images of fully hydrated and fixed specimens of skin, tendon, and cartilage and found that the fibrillar morphology was similar with comparable associated shrinking (unpublished data).

Experimental Microscope Setup

Sections were mounted onto slides and imaged with a SHG microscope consisting of a laser scanning unit (Fluoview 300, Olympus; Center Valley, PA) coupled to a mode-locked Titanium Sapphire femtosecond laser (Mira, Coherent; Santa Clara, CA) with a fundamental laser excitation wavelength of 890 nm. An Electro-Optic Modulator (EOM; ConOptics, Inc; Danbury, CT) was used to control laser power. Imaging was performed with a 40x, 0.8 NA water immersion lens (Olympus LUMPlan) and a 0.9 NA condenser. This resulted in a 180 × 180 μm field of view with approximately 0.7μm lateral and 2.5μm axial resolutions, respectively. Forward (F) and backward (B) SHG components were collected simultaneously using two identical calibrated detectors (GaAsP modules; Hamamatsu; Japan), with a scanning speed of 2.71s/frame with Kalman averaging. All measurements used circular polarization to excite all fiber orientations equally, where this was achieved at the focus through the use of a variable retarder (half wave plate) and a quarter waveplate on the optical table (18). The 445 nm SHG wavelength was verified with a fiber optic spectrometer (Ocean Optics; Dunedin, FL) after isolation with a 20 nm wide bandpass filter (Semrock; Rochester, NY). The efficiency (including PMT quantum yields) of the forward and backward (epi) collection pathways were calibrated using isotropically emitting fluorescent beads, while the final polarization state was verified by a uniform ring stain of lipid vesicles with Di-8-ANEPPS (18). Three-dimensional renderings of the image stacks were performed using Imaris visualization software (Bitplane; Zurich).

3D SHG imaging measurements

We used an average of 11 sections per specimen, and each of these sections was then imaged in three different places and the results averaged together. Those averaged values of each sample were then organized into zones based off of the depth per sample (using histological standards). The measured SHG directional (F/B ratios) values were determined by integration of the intensity of 5-10 frames per optical section every few microns of depth using ImageJ software (http://rsb.info.nih.gov/ij/). The measured attenuation, i.e. rate of intensity decrease with increasing depth into tissue, of the forward SHG signal is also used to characterize structural changes in the cartilage. Since tissues have intrinsic heterogeneity in concentration, we have found a normalized approach to the attenuation necessary to account for variability in SHG intensities in the same tissue (different fields) and to make relative comparisons between tissues (37). To this end the data of each optical series for each biopsy is self-normalized to the optical section with the average maximum intensity. The normalized forward attenuation data was taken concurrently with the F/B data.

Bulk Optical Property Measurements and Monte Carlo Simulations

The scattering anisotropy, $g,$ and the scattering coefficient, μ_s, have successfully characterized structural changes of the ECM in normal and cancerous tissues (19), and here we apply these metrics to characterize the histological zones of articular cartilage. The scattering coefficient is essentially a measure of density, as the inverse corresponds to the mean free path, or the distance a photon will travel before experiencing a collision. The scattering anisotropy, g, is associated with scattering directionality and structural organization of the tissue on a scale from 0 to 1, where these limits correspond to the following: $g = 0$, for isotropic scattering of more randomly organized structures; and $g = 1$, for highly ordered and all forward-directed scattering. The bulk optical parameters were determined at both 890 nm laser excitation and 445 nm SHG wavelengths, using the respective fundamental and frequency doubled wavelengths from the ti:sapphire laser. The bulk measurement setup followed the same protocol as previously described by Hall (38), which allows independent determination of μ_s, and g, yielding the merged parameter of the reduced scattering coefficient, $\mu_s{}'$, where:

$$\mu_s{}' = \mu_s \left(1 - g\right). \quad (3)$$

Here the values of the scattering coefficient, μ_s, are determined by on-axis attenuation measurements through the Beer-Lambert law (38):

$$I = \alpha I_0 \quad e^{-d(\mu s + \mu a)} \quad (4)$$

where I = transmission without the sample, I_0 = transmission with the sample, α = factor for losses due to refractive index mismatches (calculated to be 93%), d = tissue thickness, μ_s = scattering coefficient, and μ_a = the absorption coefficient. As $\mu_a << \mu_s$ for collagen rich tissues, it can be considered negligible and was not used for these measurements.(37) The anisotropy g is then determined by goniometry, where the angular distribution of increasing scattered light is measured from 0 to 180° through the use of a rotating photodiode detector on a motorized stage and fit to the Henyey-Greenstein (HG) phase function:

$$P(\theta) = a \frac{1 - g^2}{\left(1 + g^2 - 2g cos\theta\right)^{3/2}} \quad (5)$$

Additionally, we used the Monte Carlo simulation framework we previously developed(37) (based on multi-layered Monte Carlo (MCML)),(39) to obtain the F_{SHG}/B_{SHG} (creation ratio) with the reduced scattering coefficient μ_s', (Eq 4) from the measured F/B vs depth data..

Statistical Analysis

One-way analysis of variance (ANOVA) with Fisher's Least Significant Difference post-hoc tests were performed for F/B ratios and forward SHG attenuation (normalized by power) of all specimens. P-value less than 0.05 were considered statistically significant. These statistical analyses were performed in KaleidaGraph (Synergy Software; Reading, PA). The statistical analysis of the extracted F_{SHG}/B_{SHG} creation ratios and μ_s' from the Monte Carlo simulations was completed using a non-parametric Friedman's two-way analysis in SAS (SAS Institute, Cary, NC). Ranks were used to account for the inter-animal variability. Origin was used for graphing. (OriginLab; Northhampton, MA).

Results

Assessment of Morphology and cell distributon in ECM by SHG

As there have been many fewer publications of 3D imaging of Col II in cartilage compared to the more numerous reports imaging Col I containing tissues, we begin by comparing the appearance of these two isoforms in the SHG microscope. Figure 2 (a) and (b) show single optical sections of tendon (Col I) and patella (Col II) taken under the same imaging conditions of magnification (40x) and resolution (0.8). Note the Col I in tendon has clear, discrete fibers, and this behavior is seen in essentially all tissues comprised of this isoform (17). The appearance of Col II is visually distinct, and while it has some identifiable fibrillar architecture, it lacks the same clear appearance of long, discrete fibers seen for Col I containing tissues. We further note that the appearance of cartilage is similar even at higher resolution and magnification. This appearance makes the implementation of standard quantitative image analysis (e.g. fiber length and width) difficult. We also place this in context of the histology image of this specimen (Fig 2(c)), where the collagen lacks any clear fibrillar aspects.

We next show representative image data of the superficial transitional (STZ; 10-20% sample thickness), middle zone (40-60% sample thickness) and deep regions (70-100% sample thickness) of a patellar cartilage, as defined by histology (1-3). As there are transitions between different histological zones, there is some overlap between zonal classifications within these 100 μm thick sections. In Figure 3, the SHG images (forward and backward) of two regions in the STZ are shown, along with the 3D rendering, where some fibrillar structure is seen throughout the 100 micron axial extent of the section. The analogous image data for the middle and deep zones are shown in Figures 4 and 5, where SHG shows the Col II structure throughout these tissue sections. We note that there is some apparent alignment of the collagen fibers in the 600 μm depth, which is not observed by histology or polarized

light. The region from 1200 μm shown in Figure 5 is the beginning of the calcified region below the deep zone and clearly shows the tidemark 5 (arrow in right panel) that is typically seen in high magnification stained histology slides. The significance of seeing the tidemark lies in its potential use in pathology assessment, as infiltration of the tidemark and multiple tidemarks are signs of late OA (40).

We attempted to quantify the collagen alignment in these zones using the CT-FIRE algorithm that extracts fiber geometry from within tissues (41);however, due to the lack of sufficiently discrete Col II fibers, we were not able to quantify regions that had some visually apparent alignment. Nonetheless, we can still use the SHG images of Col II for context to probe the cell morphology (observed as holes in the images) within the different zones. The average size and shapes are given in Table 1. The cells in the STZ zone were larger and more elliptical than those in the middle and deep zones, where these differences were significant (p<0.05). The cell sizes and shapes were not significantly different between the middle and deep zones. We do not know the cause of this, but it may be due to different alignment of the short fibers over small size scales which we cannot currently quantify. We do note that this information would not be possible with the use of thin histological sections, which are on the order of thickness of single cells, and cutting can lead to elliptical appearances of even round cells. The sections used here are ~100 microns and have many layers of cells from which to sample.

SHG Directional Measurements

Measured F/B Ratio—To quantitatively compare the collagen architecture in the three zones, we measured the forward-backward ratio as a function of depth. This response arises from a coupling of the SHG emission direction F_{SHG}/B_{SHG} (described in the Introduction) and scattering governed by the reduced scattering coefficient μ_s' at λ_{SHG}. Figure 6 shows measured F/B vs. depth ratios for the three individual cartilage specimens (a, b, and c) per histological zone within each. After thresholding, the intensities were integrated over the whole field of view for three series of experiments per cartilage slice. For all cartilage zones, the F/B ratio increases with depth, which must occur according to photon diffusion theory, as there are fewer scattering events following excitation deeper within a tissue section (39).

The overall trend is that the F/B ratio is significantly higher for the middle zone compared to the STZ and deep zones, respectively, and the STZ F/B ratio is significantly higher than the deep zone (see p values in Table 2). Based on photon counting statistics, the error in the measurement is approximately 10-20%. Thus relatively small differences in F/B (e.g. 2 vs 3) are significant, even with the small data sets used here. These results are indicative of differences in fiber organization, as the F/B measurements arises from the SHG process as well as scattering, both of which are dependent on nano/microarchitecture. We will further analyze these curves below by Monte Carlo simulation.

SHG Attenuation Measurements—We point out that while the trends of the F/B vs depth ratios of the different zones shown in Figure 6 are similar, the absolute values of the F/B vary somewhat between specimens. This likely occurs due to differences in collagen concentration, cartilage heterogeneity between different animals (i.e. natural curvature,

weight of animal, exercise, etc.), and slight variations in sample thickness due to sectioning errors. We can utilize a different metric that is not subject to such specimen variability. Our approach here is to determine the normalized SHG intensity as a function of depth for each zone, where we define this response as the forward SHG attenuation. We have previously used this metric and shown it arises from the initial SHG intensity and scattering of the laser. (42) We will show below that scattering is fairly comparable between zones, and this metric will thus assess the relative brightness of each zone.

The self-normalized (including laser power) average of all the series (3 per tissue section) for each cartilage zone of all specimens is shown in Figure 7. In contrast to the F/B response, the forward SHG attenuation data does not visually show a clear distinction between histological zones. However, there is a distinct, step-wise nature in the response from the STZ zone. This was evident in all the specimens and does not appear to be an artifact, and we suggest it is related to physical structure. This may be attributed to index of refraction changes created by the transition into the middle zone as well as the interaction of the collagen matrix with the pericellular matrix and lacunae, which has been shown to produce SHG contrast (35, 43). The physical underpinning is that adjacent areas of different refractive index will have increased local scattering, as scattering is caused by refractive index mismatch at boundaries. We have shown that the forward SHG is largely governed by the loss of the laser squared due to scattering(37). Thus, local increased scattering will decrease the measured SHG. We previously observed an analogous response in skeletal muscle tissue, where the muscle cells are wrapped by higher refractive index collagen perimysium (1.45 vs 1.38). Similar steps were found at the muscle cell boundaries, and we saw these oscillations approximately at 20 micron intervals, which was the size of the muscle cells shown in x-z projections (42).

Bulk Optical Parameter Measurements

To the best of our knowledge there is essentially no published data on bulk optical properties on cartilage, and certainly not in the context of the different zones. Here we measured the scattering coefficient μ_s, which physically corresponds to density, and the scattering anisotropy, g, which is reflective of organization.

Scattering Coefficient—The scattering coefficient, μ_s, for all three zones at both the excitation and SHG wavelength are given in Table 3. We were only able to perform these measurements on two samples, and cannot claim statistical significance. Thus the values are for mainly for comparison with literature values on other collagen rich ECM tissues. We have found the error of these measurements to be about 5%.

For all zones the scattering coefficients are approximately 2 fold higher at the SHG (445 nm) than the excitation wavelength (890 nm), where this wavelength dependence is typical of collagen ECM (44, 45). These absolute values are also similar to those we have reported for other collagenous tissues, such as skin and ovary (19, 37). At 445 nm, the deep zone scattering coefficient is slightly higher than both the middle and STZ zones; however, the middle zone is similar to the STZ. At 890 nm, the deep zone scattering coefficient is higher than the STZ and middle zones, and the middle zone is more scattering than the STZ. As μ_s

is reflective of overall density, where for the patella this is a combined effect of the collagen, GAGS, and cells, this suggests the deep zone has the highest density.

Scattering Anisotropy—The scattering anisotropy, *g*, is associated with structural organization and scattering directionality of the tissue, is calculated through a combination of on-axis attenuation measurements and goniometry(38) The resulting values for all three zones and at both wavelengths were between 0.91 and 0.93. None of the values were different (see Table 3). While not different between the zones, these values are also similar to those of other collagen rich ECM tissues (45).

F_{SHG}/B_{SHG} Creation Ratio

We next further analyze the F/B data vs depth data (Figure 6), where the measured response is a coupling of the SHG creation ratio, F_{SHG}/B_{SHG}, and scattering governed by the reduced scattering coefficient, μ_s'. Since these components are experimentally indistinguishable, we must use Monte Carlo simulations to decouple the underlying sources. We have previously implemented two different approaches to this solution (37, 45). Here we use the method in Ref. #45 that simultaneously obtains both the SHG creation ratio and reduced scattering coefficient at λ_{SHG}. The data and optimal simulation for each zone are shown in Figure 8, where only widely separated simulated points are shown for ease of viewing. In each case, the data and simulation were not statistically different based, providing confidence in the results of the analysis. The resulting values for F_{SHG}/B_{SHG} and μ_s' are shown in Table 4. The middle zone creation ratio is significantly higher than the deep (p = 0.002) and the STZ (p = 0.02) zones, respectively. The creation ratio was also different for the STZ and deep zones (p=0.02).

The reduced scattering coefficients for the three zones were not statistically different through this analysis, although the bulk optical determination of the scattering coefficient (Table 2) suggested higher scattering in the deep zone. The reduced scattering coefficients were approximately similar for both measurements, and similar to our previous measurements on tendon and the ovarian stroma (45). We note the reduced scattering coefficient, μ_s', and the scattering coefficient, μ_s refer to different properties. The latter is essentially a measure of density, whereas the former is a merged parameter arising from density and organization. Thus, it is possible for one parameter to have statistically different behavior than the other. We are investigating the underlying physical properties that give rise to the results here.

Discussion

The goal of this work was to characterize the different histological zones of articular cartilage using SHG imaging, measurement of optical properties and Monte Carlo simulation analysis to understand the ECM changes in normal tissue in order to have a baseline for future normal and disease comparisons. While there have been a few efforts using SHG to image cartilage (29, 31), these have not yet exploited the full power of the modality in terms of extracting structure (16, 20). There is also limited data on optical properties.

Analysis of fiber size and alignment of Col II fibers is difficult, as while fibrillar, the fibers are short and not always discrete on these size scales, in large contrast to Col I (see Fig 2). For example, the CT-FIRE algorithm was unsuccessful in determining overall alignment or alignment around cells. We also attempted the use of 2D-FFTs, but this resulted in little delineation between zones. We further attempted a form of texture analysis using 2D wavelet transforms with Principal Components Analysis (PCA) with KNN nearest neighbor classification, which we recently reported for analysis of images of idiopathic pulmonary fibrosis (46). This approach, like the FFT was also unsuccessful here. We note that this is striking contrast to Col I fibers which appear much sharper even at the same resolution, and these analyses are often successful. Thus, different tools are necessary for quantitative assessment of the fibrillar architecture in hyaline cartilage.

We previously developed the method of 3D measurements of the SHG directional response, bulk optical properties, coupled with Monte Carlo simulation analysis approach as a general method to quantify tissue structure. Specially, sub-resolution features are manifested in the SHG creation ratio (F_{SHG}/B_{SHG}) (23) where this correlates with fibril packing, and a larger creation ratio is related more organized fibril packing on the sizescale of λ_{SHG}. The bulk optical properties are also related to tissue structure. We have used this combined approach for many different tissues, including skin, tendon, muscle, and ovarian stroma. We have also used the F/B and attenuation measurement in fibrillary models of Col I/Col V (breast cancer model) and Col I and Col III (ovarian cancer model). Here we used this tactic to reveal differences in assembly in the superficial, middle and deep zones. We previously developed a heuristic model to explain trends in the SHG creation ratio based on the packing relative to λ_{SHG} (23). Within this framework, the higher SHG creation ratio, F_{SHG}/B_{SHG} measured from the middle zone is reflective of more organized sub-resolution fibril structure. We note that this collagen specific finding is in large contrast to the conventional histological picture.

We were unable to perform optical scattering measurements on all of the specimens due to tissue degradation, and could not obtain significance. As we could not locate zone specific optical property values in the literature, it useful to have even preliminary documentation of these structural metrics. We observed a trend that the deep region was slightly more scattering than the STZ and middle zone. This is consistent with the deep zone being near the calcified region and having higher density. The extracted reduced scattering coefficient, μ_s', determined through the Monte Carlo simulations was only slightly higher as well. The differences in measured F/B vs depth data in Figure 6, which were all significant, can then be ascribed to differences in the SHG creation ratio, F_{SHG}/B_{SHG}, which is reflective of the sub-resolution fibril structure. These metrics are important as these structural properties could likely change during in diseased states or effects of aging. It is important to measure these at different wavelengths as this dependence is further related to tissue structure. For example, a weaker spectral dependence of optical scattering is interpreted as arising from a more ordered structure(47) . Thus these can be considered biomarkers, adding further information to the SHG imaging. Our Monte Carlo simulation code for both SHG and optical property determination is available upon request.

Because of the structural capabilities, SHG is more powerful in probing the collagen fiber network than PLM and EM in several ways. First, it provides the ability to provide optical

sectioning in imaging a thick, unfixed and intact sample in an *en face* geometry. In contrast, the majority of the previous cartilage imaging studies have used 5 μm thick, paraffin-embedded histological sagittal sections. This is important as more data can be obtained from the tissue, which is critical in patella due to the intrinsic heterogeneity even within the zones. Second, through the use of staining, it is not possible to view the collagen fibers, only the overall collagen content. This is where SHG has clear advantages over histology even in visualization of thin sections. Third, polarized light microscopy (PLM) uses linear birefringence to assess the collagen fiber orientations, which can only be performed on thin sections in between cross polarizers and cannot determine molecular organization. SHG also results, in part from birefringence, but the contrast mechanism is more complicated than the pure linear birefringence in PLM. We previously have compared these contrast mechanisms directly in imaging *C. elegans* and discussed similarities and differences. (16) While not used here, polarization resolved SHG can extract both macromolecular and supramolecular structural aspects through using all combinations of excitation and signal polarization.(48) Of specific relevance to the current work, the F/B analysis is specific and unique to SHG as it arises from the coherence of the process, and there is no classical optical microscopy analog.

Future work will utilize these polarization analyses along with the methods reported here to study changes in fibrillar architecture in OA and other diseases. We will also attempt to use other 2D texture analysis to differentiate the zones based on the fiber morphology. Such studies would allow better correlation of the alignment and organization seen by SHG with previous determinations through histology, PLM and μMRI (2, 11, 12).

Conclusions

This exploratory study has identified a collection of physical/structural properties of the ECM that changes throughout the depth of articular cartilage. In this effort, we have identified SHG signatures that are different between the different histological zones of articular cartilage. Specifically, through SHG imaging and Monte Carlo simulation analysis we found depth-dependent attenuation and directional responses that are consistent with many of the differences in tissue structure previously shown by histological and macro-scale imaging modalities. In particular, the zone dependent spatial relationship of collagen and cells is also seen by SHG. In addition, through SHG these signatures of structure are seen at both the fiber and fibril levels of assembly. Of note, through SHG characterization we found the middle zone to have the most organized structure, which is in strong contrast to most histological data. Our longer term goals are to use these structural changes in the ECM as a specific biomarker in different diseased states of OA in order to better appreciate the confounding disease pathogenesis and eventually expand from the current technological state of *ex vivo/in vitro* to *in vivo* applications.

Acknowledgments

References

1. Buckwalter JA, Mow VC, Ratcliffe A. Restoration of Injured or Degenerated Articular Cartilage. J Am Acad Orthop Surg. Jul; 1994 2(4):192–201. [PubMed: 10709009]

2. Pearle AD, Warren RF, Rodeo SA. Basic science of articular cartilage and osteoarthritis. Clin Sports Med. Jan; 2005 24(1):1–12. [PubMed: 15636773]

3. Sophia Fox AJ, Bedi A, Rodeo SA. The basic science of articular cartilage: structure, composition, and function. Sports Health. Nov; 2009 1(6):461–8. [PubMed: 23015907]

4. Squires GR, Okouneff S, Ionescu M, Poole AR. The pathobiology of focal lesion development in aging human articular cartilage and molecular matrix changes characteristic of osteoarthritis. Arthritis Rheum. May; 2003 48(5):1261–70. [PubMed: 12746899]

5. Poole AR, Kobayashi M, Yasuda T, Laverty S, Mwale F, Kojima T, et al. Type II collagen degradation and its regulation in articular cartilage in osteoarthritis. Ann Rheum Dis. Nov; 2002 61(Suppl 2):ii78–81. [PubMed: 12379630]

6. Wu W, Billinghurst RC, Pidoux I, Antoniou J, Zukor D, Tanzer M, et al. Sites of collagenase cleavage and denaturation of type II collagen in aging and osteoarthritic articular cartilage and their relationship to the distribution of matrix metalloproteinase 1 and matrix metalloproteinase 13. Arthritis Rheum. Aug; 2002 46(8):2087–94. [PubMed: 12209513]

7. Lippiello L, Hall D, Mankin HJ. Collagen synthesis in normal and osteoarthritic human cartilage. J Clin Invest. Apr; 1977 59(4):593–600. [PubMed: 845251]

8. Billinghurst RC, Dahlberg L, Ionescu M, Reiner A, Bourne R, Rorabeck C, et al. Enhanced cleavage of type II collagen by collagenases in osteoarthritic articular cartilage. J Clin Invest. Apr 1; 1997 99(7):1534–45. [PubMed: 9119997]

9. Hollander AP, Pidoux I, Reiner A, Rorabeck C, Bourne R, Poole AR. Damage to type II collagen in aging and osteoarthritis starts at the articular surface, originates around chondrocytes, and extends into the cartilage with progressive degeneration. J Clin Invest. Dec; 1995 96(6):2859–69. [PubMed: 8675657]

10. Campagnola, PJ. Second Harmonic Generation Imaging Microscopy of Structural Protein Arrays in Tissue. In: Masters, BR.; So, PTC., editors. Handbook of Biomedical Nonlinear Optical Microscopy. Oxford University Press; Oxford, NY: 2008. p. 377-411.

11. Nieminen MT, Rieppo J, Töyräs J, Hakumäki JM, Silvennoinen J, Hyttinen MM, et al. T2 relaxation reveals spatial collagen architecture in articular cartilage: a comparative quantitative MRI and polarized light microscopic study. Magn Reson Med. Sep; 2001 46(3):487–93. [PubMed: 11550240]

12. Xia Y, Moody JB, Burton-Wurster N, Lust G. Quantitative in situ correlation between microscopic MRI and polarized light microscopy studies of articular cartilage. Osteoarthritis Cartilage. Jul; 2001 9(5):393–406. [PubMed: 11467887]

13. Raya JG, Arnoldi AP, Weber DL, Filidoro L, Dietrich O, Adam-Neumair S, et al. Ultra-high field diffusion tensor imaging of articular cartilage correlated with histology and scanning electron microscopy. MAGMA. Aug; 2011 24(4):247–58. [PubMed: 21630094]

14. Kourkoutis, LF.; Plitzko, JM.; Baumeister, W. Electron Microscopy of Biological Materials at the Nanometer Scale. In: Clarke, DR., editor. Annual Review of Materials Research. Vol. 42. Annual Reviews; Palo Alto: 2012. p. 33-58.

15. Michler GH. Problems Associated with the Electron Microscopy of Polymers. Electron Microscopy of Polymers: Springer Berlin Heidelberg;. 2008:175–83.

16. Campagnola PJ, Millard AC, Terasaki M, Hoppe PE, Malone CJ, Mohler WA. Three-dimensional high-resolution second-harmonic generation imaging of endogenous structural proteins in biological tissues. Biophys J. Jan.2002 82:493–508. 1 Pt 1. [PubMed: 11751336]

17. Campagnola P. Second harmonic generation imaging microscopy: applications to diseases diagnostics. Anal Chem. May 1; 2011 83(9):3224–31. [PubMed: 21446646]

18. Chen X, Nadiarynkh O, Plotnikov S, Campagnola PJ. Second harmonic generation microscopy for quantitative analysis of collagen fibrillar structure. Nature protocols. Apr; 2012 7(4):654–69. [Research Support, N.I.H., Extramural]. [PubMed: 22402635]

19. Nadiarnykh O, LaComb RB, Brewer MA, Campagnola PJ. Alterations of the extracellular matrix in ovarian cancer studied by Second Harmonic Generation imaging microscopy. BMC Cancer. 2010; 10:94. [PubMed: 20222963]

20. Campagnola PJ, Loew LM. Second-harmonic imaging microscopy for visualizing biomolecular arrays in cells, tissues and organisms. Nat Biotechnol. Nov; 2003 21(11):1356–60. [PubMed: 14595363]

21. Plotnikov SV, Millard AC, Campagnola PJ, Mohler WA. Characterization of the Myosin-based source for second-harmonic generation from muscle sarcomeres. Biophys J. Jan; 2006 90(2):693–703. [PubMed: 16258040]

22. Mohler W, Millard AC, Campagnola PJ. Second harmonic generation imaging of endogenous structural proteins. Methods. Jan; 2003 29(1):97–109. [PubMed: 12543075]

23. Lacomb R, Nadiarnykh O, Townsend SS, Campagnola PJ. Phase Matching considerations in Second Harmonic Generation from tissues: Effects on emission directionality, conversion efficiency and observed morphology. Opt Commun. Apr 1; 2008 281(7):1823–32. [PubMed: 19343083]

24. Williams RM, Zipfel WR, Webb WW. Interpreting second-harmonic generation images of collagen I fibrils. Biophys J. Feb; 2005 88(2):1377–86. [PubMed: 15533922]

25. Legare F, Pfeffer C, Olsen BR. The Role of Backscattering in SHG Tissue Imaging. Biophys J. Aug 15; 2007 93(4):1312–20. [PubMed: 17449666]

26. Pfeffer CP, Olsen BR, Ganikhanov F, Légaré F. Multimodal nonlinear optical imaging of collagen arrays. J Struct Biol. Oct; 2008 164(1):140–5. [PubMed: 18664383]

27. Mansfield JC, Winlove CP, Moger J, Matcher SJ. Collagen fiber arrangement in normal and diseased cartilage studied by polarization sensitive nonlinear microscopy. J Biomed Opt. Jul-Aug; 2008 13(4):044020. [PubMed: 19021348]

28. Mansfield JC, Winlove CP. A multi-modal multiphoton investigation of microstructure in the deep zone and calcified cartilage. J Anat. Apr; 2012 220(4):405–16. [PubMed: 22332832]

29. Brockbank KG, MacLellan WR, Xie J, Hamm-Alvarez SF, Chen ZZ, Schenke-Layland K. Quantitative second harmonic generation imaging of cartilage damage. Cell Tissue Bank. Dec; 2008 9(4):299–307. [PubMed: 18431689]

30. Lilledahl MB, Pierce DM, Ricken T, Holzapfel GA, Davies CeL. Structural analysis of articular cartilage using multiphoton microscopy: input for biomechanical modeling. IEEE Trans Med Imaging. Sep; 2011 30(9):1635–48. [PubMed: 21478075]

31. Brown CP, Houle MA, Chen M, Price AJ, Légaré F, Gill HS. Damage initiation and progression in the cartilage surface probed by nonlinear optical microscopy. J Mech Behav Biomed Mater. Jan; 2012 5(1):62–70. [PubMed: 22100080]

32. Brown CP, Houle MA, Popov K, Nicklaus M, Couture CA, Laliberté M, et al. Imaging and modeling collagen architecture from the nano to micro scale. Biomed Opt Express. Dec; 2013 5(1):233–43. [PubMed: 24466490]

33. Werkmeister E, de Isla N, Marchal L, Stoltz JF, Dumas D. Interest of second harmonic generation imaging for diagnosis in thick and opaque tissue. Biorheology. 2008; 45(3-4):375–83. [PubMed: 18836238]

34. Yeh AT, Hammer-Wilson MJ, Van Sickle DC, Benton HP, Zoumi A, Tromberg BJ, et al. Nonlinear optical microscopy of articular cartilage. Osteoarthritis Cartilage. Apr; 2005 13(4):345–52. [PubMed: 15780648]

35. Werkmeister E, de Isla N, Netter P, Stoltz JF, Dumas D. Collagenous extracellular matrix of cartilage submitted to mechanical forces studied by second harmonic generation microscopy. Photochem Photobiol. Mar-Apr;2010 86(2):302–10. 2010. [PubMed: 19930118]

36. Meek KM. The use of glutaraldehyde and tannic acid to preserve reconstituted collagen for electron microscopy. Histochemistry. 1981; 73(1):115–20. [PubMed: 6797991]

37. Lacomb R, Nadiarnykh O, Campagnola PJ. Quantitative SHG imaging of the diseased state Osteogenesis Imperfecta: Experiment and Simulation. Biophys J. 2008; 94:4504–14. [PubMed: 18281387]

38. Hall G, Jacques SL, Eliceiri KW, Campagnola PJ. Goniometric measurements of thick tissue using Monte Carlo simulations to obtain the single scattering anisotropy coefficient. Biomedical Optics Express. Nov 1; 2012 3(11):2707–19. [PubMed: 23162710]

39. Wang L, Jacques SL, Zheng L. MCML--Monte Carlo modeling of light transport in multi-layered tissues. Comput Methods Programs Biomed. Jul; 1995 47(2):131–46. [PubMed: 7587160]

40. Madry H, Luyten FP, Facchini A. Biological aspects of early osteoarthritis. Knee Surg Sports Traumatol Arthrosc. Mar; 2012 20(3):407–22. [Research Support, Non-U.S. Gov't Review]. [PubMed: 22009557]

41. Bredfeldt JS, Liu Y, Pehlke CA, Conklin MW, Szulczewski JM, Inman DR, et al. Computational segmentation of collagen fibers from second-harmonic generation images of breast cancer. J Biomed Opt. Jan.2014 19(1):16007. [PubMed: 24407500]

42. LaComb R, Nadiarnykh O, Carey S, Campagnola PJ. Quantitative SHG imaging and modeling of the optical clearing mechanism in striated muscle and tendon. J Biomed Opt. 2008; 13:021108. [PubMed: 18465957]

43. Mansfield J, Yu J, Attenburrow D, Moger J, Tirlapur U, Urban J, et al. The elastin network: its relationship with collagen and cells in articular cartilage as visualized by multiphoton microscopy. J Anat. Dec; 2009 215(6):682–91. [Research Support, Non-U.S. Gov't]. [PubMed: 19796069]

44. Hall G, Tilbury KB, Campbell KR, Eliceiri KW, Campagnola PJ. Experimental and simulation study of the wavelength dependent second harmonic generation of collagen in scattering tissues. Optics Letters. Apr 1; 2014 39(7):1897–900. [PubMed: 24686633]

45. Hall G, Eliceiri KW, Campagnola PJ. Simultaneous determination of the second-harmonic generation emission directionality and reduced scattering coefficient from three-dimensional imaging of thick tissues. J Biomed Opt. Nov 1.2013 18(11):116008. [PubMed: 24220726]

46. Tilbury K, Hocker J, Wen BL, Sandbo N, Singh V, Campagnola PJ. Second harmonic generation microscopy analysis of extracellular matrix changes in human idiopathic pulmonary fibrosis. J Biomed Opt. Aug.2014 19(8):86014.

47. Rogers JD, Capoglu IR, Backman V. Nonscalar elastic light scattering from continuous random media in the Born approximation. Optics Letters. Jun 15; 2009 34(12):1891–3. [PubMed: 19529738]

48. Tilbury K, Lien CH, Chen SJ, Campagnola PJ. Differentiation of Col I and Col III Isoforms in Stromal Models of Ovarian Cancer by Analysis of Second Harmonic Generation Polarization and Emission Directionality. Biophys J. Jan 21; 2014 106(2):354–65. [PubMed: 24461010]
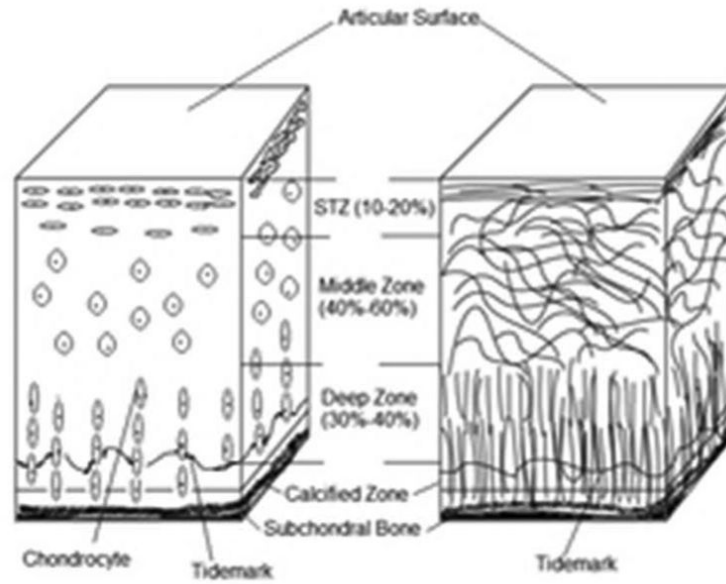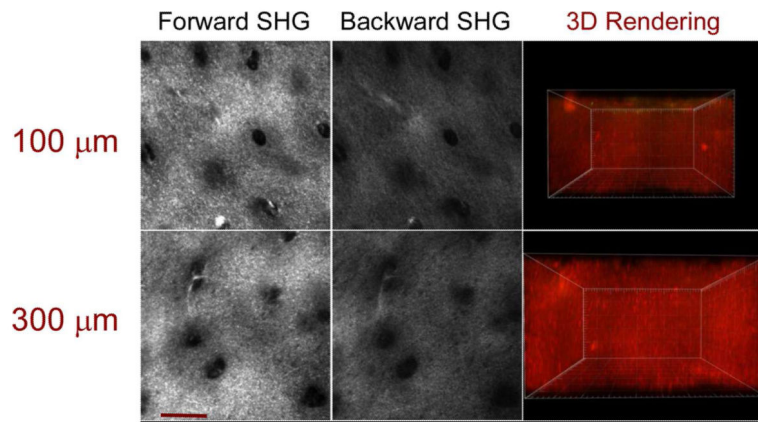
Figure 1.
Articular cartilage divided into its histological zones. This image depicts the cellular structure and organization as well as the collagen fiber orientation from surface to bone based on histological data. Note the randomness of collagen fibers in the middle zone. Figure inspired by Buckwalter et al. JAAOS, 1994; 2:192-201.
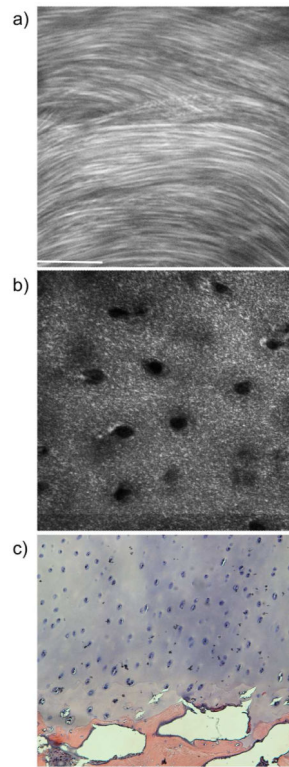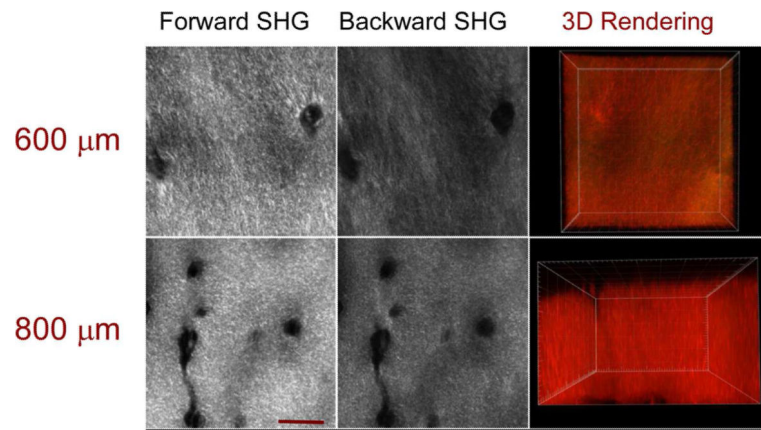
Figure 2.
Representative images of forward SHG from rat tail tendon (a) and from cartilage (b). The former is Col I and the latter Col II. The Col II fibers are not as discrete or easily identifiable as Col I. Scale bar= 40μm. The Masson trichrome is shown in 2(c), where this staining lacks any fibrillar features.

Figure 3.
Representative images of forward and backward SHG from 2 depths for the superficial zone of cartilage. The ratio of these images will be used in Fig 6. The 3D rendering of the z-stack from these images are shown at the right, showing that SHG can image the structure throughout this depth. Scale bar= 40μm.

Figure 4.
Representative images of forward and backward SHG for two depths in the middle zone of cartilage. The ratio of these images will be used in Fig 6. Unlike histology data, some oriented fibers are shown in this zone. The 3D rendering of the z-stack from these images are shown at the right, showing that SHG can image the structure throughout this depth. Scale bar=40μm.
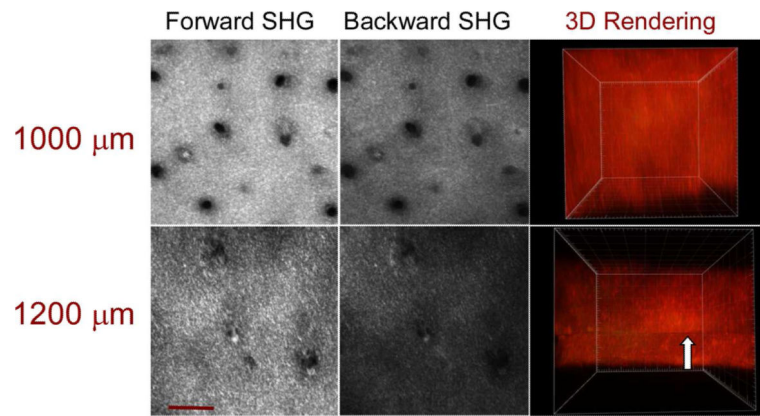
Figure 5.
Representative images of forward and backward SHG for two depths from the deep zone of cartilage. The 3D rendering of the z-stack from these images are shown at the right, showing that SHG can image the structure throughout this depth. The tidemark, indicated by the white arrow, denotes the transition between the deep zone and calcified cartilage, visualized about 1300 μm deep. Scale bar=40 μm.
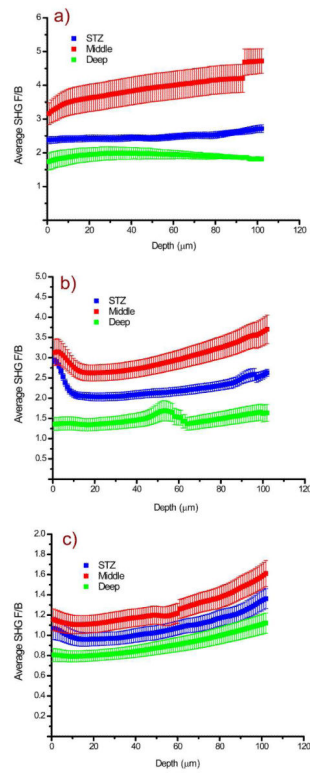
Figure 6.
Average F/B ratios and standard errors as a function of cartilage depth for the different zones for the 3 cartilage specimens. The overall trend is that the F/B ratio is highest for the middle zone, followed by the STZ and deep zones, respectively.
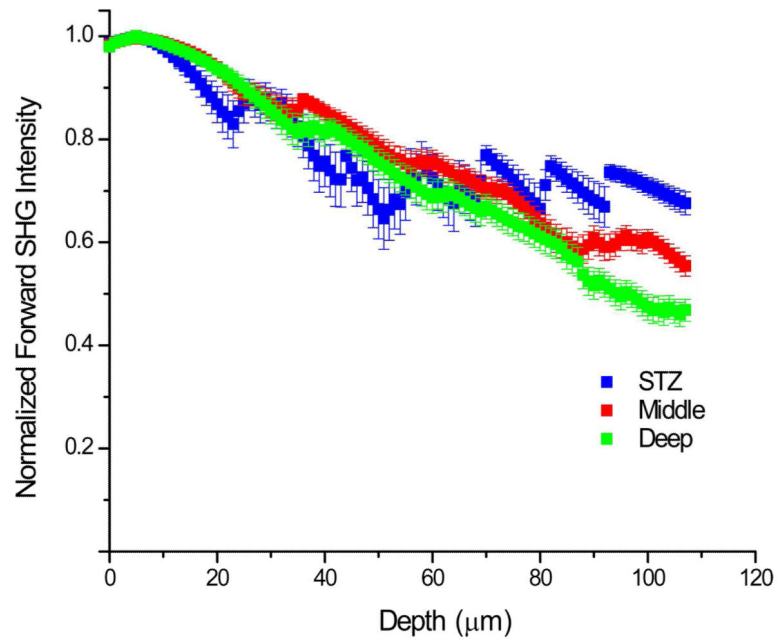
Figure 7.
Forward SHG attenuation data, normalized by power per series, of the 3 cartilage histological zones for all samples. See text for description of the step-wise behavior in the STZ.
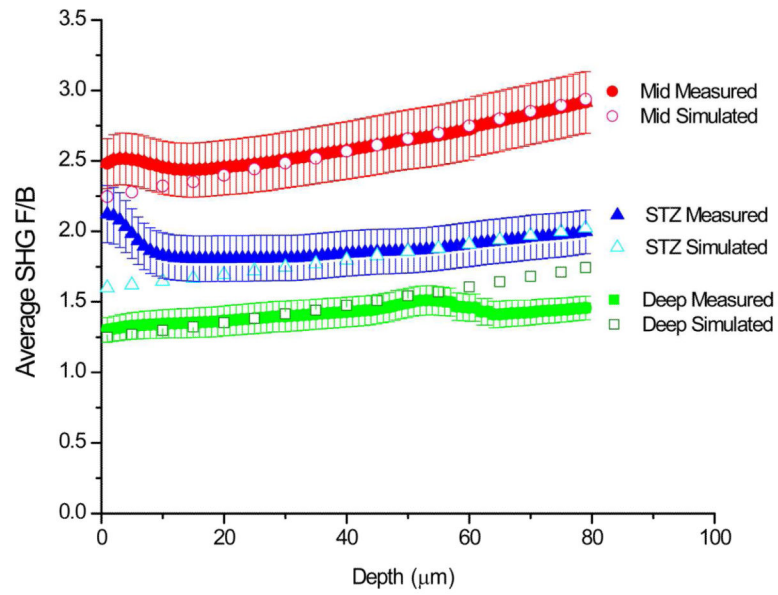
Figure 8.
Average F/B ratios and standard errors as a function of cartilage depth for the different zones for the 3 cartilage specimens with the corresponding optimal Monte Carlo simulation for the 3 the histological zones. The simulated points are shown sparsely for clarity.

Table 1

Cell geometrical properties in each zone

Histological Zone	Area (μ²)	Perimeter (μm)	Circularity (0 to 1)
STZ	124 ± 5.1	80.2 ± 3.0	0.28
Middle	72.4 ± 2.7	57.8 ± 1.6	0.33
Deep	82.9 ± 4.1	60.7 ± 1.9	0.31

Table 2

Comparisons of p values comparing the F/B ratio of the different zones of articular cartilage for each sample. The F/B ratio was significantly different for all zones per respective sample. Refer to Figure 6 for the F/B ratio data.

Sample	F/B Ratio per Zone	P-Value
1	STZ vs. Middle	<0.0001
	STZ vs. Deep	<0.0001
	Middle vs. Deep	<0.0001
2	STZ vs. Middle	<0.0001
	STZ vs. Deep	<0.0001
	Middle vs. Deep	<0.0001
3	STZ vs. Middle	<0.0001
	STZ vs. Deep	<0.0001
	Middle vs. Deep	<0.0001

Table 3

Bulk optical parameters of μ_s and *g* for all histological zones of cartilage at the laser excitation and SHG wavelengths. Values are listed as an average of bulk measured samples per zone ± standard error.

Histological Zone	λ (nm)	μ_s (n = 2) (cm^{-1})	g_{single} (n = 2)
STZ	445 890	180.1 ± 14.5 75.17 ± 6.61	0.91 0.92
Middle	445 890	183.9 ± 9.09 91.12 ± 6.62	0.91 0.93
Deep	445 890	220.0 ± 14.6 107.2 ± 8.11	0.92 0.93

Table 4

Resulting F_{SHG}/B_{SHG} creation ratio and reduced scattering coefficients from Monte Carlo simulations of the measured F/B vs depth data of the histological zones of cartilage. Values are listed as the average from the 3 samples per zone ± standard error.

Histological Zone	μ_s' (445nm) (cm^{-1})	F_{SHG}/B_{SHG} Creation Ratio
STZ	17.8 ± 3.7	2.3 ± 0.50
Middle	15.3 ± 3.6	3.8 ± 1.2
Deep	17.6 ± 1.5	1.9 ± 0.29